Shock and Vibration

WILEY

RESEARCH ARTICLE OPEN ACCESS

A Hybrid LightGBM–WOA Model for Accurate Prediction of Back-Break in Mine Blasting Operations: A Case Study

Mojtaba Yari[1] | Biao He[2] | Xuzhen He[3] | Payam Abbasi[4] | Hadi Fattahi[5] | Danial Jahed Armaghani[3] | Manoj Khandelwal[6,7,8]

[1]Department of Mining Engineering, Faculty of Engineering, Malayer University, Malayer, Iran | [2]Department of Civil Engineering, Faculty of Engineering, Universiti Malaya, Kuala Lumpur 50603, Malaysia | [3]School of Civil and Environmental Engineering, University of Technology Sydney, Ultimo 2007, New South Wales, Australia | [4]Marane Olia Ornamental Stone Mine, Sanandaj, Iran | [5]Faculty of Earth Sciences Engineering, Arak University of Technology, Arak, Iran | [6]Institute of Innovation, Science and Sustainability, Federation University Australia, Ballarat, Australia | [7]Laboratory of Sustainable Development in Natural Resources and Environment, Institute for Advanced Study in Technology, Ton Duc Thang University, Ho Chi Minh City, Vietnam | [8]Faculty of Environment and Labour Safety, Ton Duc Thang University, Ho Chi Minh City, Vietnam

Correspondence: Hadi Fattahi (h.fattahi@arakut.ac.ir) | Manoj Khandelwal (m.khandelwal@federation.edu.au); (khandelwalmanoj@tdtu.edu.vn)

Received: 11 January 2025 | **Revised:** 14 November 2025 | **Accepted:** 22 November 2025

Academic Editor: Zhipeng Zhao

Keywords: back-break | blasting operation | environmental issue | LightGBM | whale optimization algorithm

ABSTRACT

Back-break (BB), a significant environmental concern in mining operations, arises from the improper execution of blasting techniques. The primary cause of BB is the inadequate design of blasting pattern parameters, which leads to structural issues such as fractures, overhangs, and underhangs on the construction face. These issues escalate the costs associated with creating a smooth high wall and a clear face for subsequent blasts. Given the critical need to address these challenges, developing a reliable predictive model for BB is essential. Such a model can effectively represent the inherent characteristics of the construction face and guide more precise blasting operations. This study introduces an advanced predictive model leveraging a tree-based approach, light gradient boosting machine (LightGBM), optimized through the whale optimization algorithm (WOA). The unique integration of WOA in this model ensures the identification of optimal hyperparameters, enhancing the LightGBM model's predictive accuracy. The model was trained using a comprehensive dataset of BB measurements obtained from the Sungun mine in Iran, a prominent mining site known for its complex geological features. The findings from this study underscore the efficacy of the proposed hybrid LightGBM–WOA model in accurately forecasting BB. On the training dataset, the model achieved a coefficient of determination (R^2) of 0.997, a value account for (VAF) of 99.651%, and a root mean square error (RMSE) of 0.152. The model's performance on the test dataset was equally robust, with an (R^2) of 0.990, a VAF of 99.030%, and an RMSE of 0.230. These results demonstrate the model's potential to significantly improve the precision of blasting operations, thereby reducing environmental impact and operational costs.

1 | Introduction

The mining industry is one of the fundamental pillars in the development of human civilization [1]. In many countries, mining serves as the backbone of the economy, with numerous other sectors heavily reliant on it. The primary method of resource extraction, particularly in open-pit mines, is drilling and blasting, which is essential for rock fragmentation. The effectiveness of modern drilling and blasting techniques has seen significant improvements, largely due to advances in industrial

This is an open access article under the terms of the Creative Commons Attribution License, which permits use, distribution and reproduction in any medium, provided the original work is properly cited.

Copyright © 2026 Mojtaba Yari et al. *Shock and Vibration* published by John Wiley & Sons Ltd.

detonators, initiation systems, and drilling equipment [2]. However, the negative impacts of blasting, such as fly-rock, ground vibration, air overpressure, and back-break (BB) [3–5], as shown in Figure 1, must be carefully assessed, as they can have detrimental effects on surrounding areas [7].

BB is an unintended consequence of blasting operations. It occurs when unplanned breakage extends beyond the rear row of blast holes after a blasting cycle [8]. This phenomenon crushes the rock mass behind the last line of holes, which subsequently reduces the quality of drilling in the following round and negatively impacts the overall efficiency of the blasting process [9]. The most evident drawback of BB is the creation of an uneven burden (B) after the blast, which can lead to fly-rock and poor fragmentation in subsequent blasts [10]. The costs associated with mining and processing plants are directly linked to the size distribution of rock fragments [11]. Although there are methods to control the extent and boundaries of blasting-induced BB, these techniques are often expensive and time-consuming [2]. Line drilling, cushion blasting, and presplitting are among the most well-known controlled blasting techniques used to reduce BB [12].

To provide a clear perspective on the methodologies available for estimating BB, previous studies have been reviewed, revealing that the techniques in this field can be categorized into three main groups: (i) empirical, (ii) statistical and probabilistic, and (iii) machine learning (ML). In empirical models, the maximum charge per delay and the distance between the monitoring point and the free face are two critical factors. Lundborg [13] and Roth [14] introduced several empirical models for predicting BB. However, these models face significant limitations [15]: (1) they rely on only two input parameters, (2) they can predict only one output at a time, and (3) they are not applicable to different geological formations or mining conditions [6]. Consequently, researchers are increasingly adopting newer models that can simultaneously account for the numerous factors influencing blasting outcomes.

Many studies have employed statistical methods to predict blasting-induced BB. For instance, Sharma et al. [16] utilized a multivariate regression model, while Esmaeili et al. [17] developed a multiple regression model for this purpose. Esmaeili and colleagues found that statistical models generally perform worse than advanced ML models. In exploring probabilistic methods, Sari et al. [18] assessed the suitability of stochastic modeling and evaluated the significance of controllable factors on BB using the Monte Carlo method. Their findings indicated that stochastic modeling can be effectively used to model and analyze the impact of various blasting parameters on BB. However, several researchers have noted that statistical and probabilistic models tend to have lower accuracy compared to ML models [17, 19]. The poor performance of these models is attributed to the complex interactions between the numerous influencing factors, leading to oversimplified assumptions [20].

In recent years, numerous scholars have demonstrated that ML can be effectively employed in many regression, classification and time-series problems of civil and geotechnical engineering [21–24]. Ziaie et al. [25] proposed a hybrid tree-based model to predict liquefaction-induced lateral displacements and found a high accuracy of this model, where they used only four key soil parameters. Another hybrid artificial neural network (ANN) model was introduced to predict tunnel construction rate in the study conducted by Armaghani et al. [26]. In another study, Asteris et al. [27] presented an ANN model that accurately predicts rock strength from nondestructive tests. In the area of blasting side effects, there are many studies that highlight the successful use of ML techniques [28–30]. Ghasemi et al. [31] developed a predictive model for BB using an adaptive neuro-fuzzy inference system, achieving very promising results. Saghatforoush et al. [32] successfully predicted and optimized BB by combining neural networks with ant colony optimization algorithms. Kumar et al. [33] applied the random forest (RF) method to predict BB, achieving a coefficient of determination (R^2) of 0.979 and a root mean square error (RMSE) of 0.879, demonstrating the RF model's strong predictive capability. These studies clearly indicate that ML models outperform the other two approaches in predicting blasting-induced BB.

In this study, a highly accurate prediction of BB was achieved by training a tree-based model, specifically the Light gradient boosting machine (LightGBM) model, using data collected from the Sungun copper mine in Iran. LightGBM, along with other ML models, has been recognized for its power and versatility in various sectors of civil and mining engineering [34, 35]. To

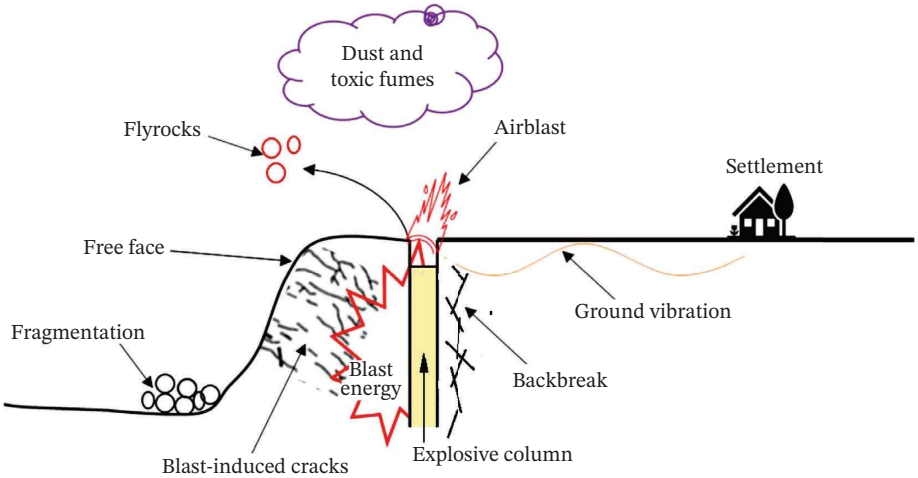


FIGURE 1 | The most undesirable side effects of blasting-induced operations [6].

3148, 2026, 1, Downloaded from https://onlinelibrary.wiley.com/doi/10.1155/vib/4973137 by National Health And Medical Research Council, Wiley Online Library on [18/11/2026]. See the Terms and Conditions (https://onlinelibrary.wiley.com/terms-and-conditions) on Wiley Online Library for rules of use; OA articles are governed by the applicable Creative Commons License

optimize the LightGBM model's hyperparameters, a robust optimization technique known as the whale optimization algorithm (WOA) was employed. The WOA enhances the model's potential to achieve optimal performance. In the final stage, the Shapley Additive Explanations (SHAP) method was applied to analyze the relationships between the influencing factors and BB. This approach provides deeper insight into the precise impact of each input factor on BB occurrence.

2 | Case Study and Data Collection

The Sungun mine (Figure 2) is the largest open-pit copper mine in northwestern Iran [37]. Located approximately 125 km north of Tabriz, the capital city of East Azarbaijan province, the mine is situated at latitude 38°38′20″ N and longitude 46°45′35″ E. The semicircular pit of the Sungun mine features high walls on three sides, with a lower wall to the east. The mine's elevation is around 2000 m.

The oldest mineralized intrusive body at the Sungun mine is quartz-monzonite, dating back to the Early Miocene [38]. These rocks are part of the Sahand-Bazman orogenic belt of the Cenozoic era. The geology is further characterized by a suite of porphyritic granitoids and late dikes that intersect the Oligo-Miocene andesite and upper Cretaceous limestone [39]. While copper is the primary mineral, several secondary minerals are also present, including chalcopyrite, malachite, pyrite, chalcocite, and cuprite. The deposit's grade increases with depth, and valuable elements such as gold, silver, and molybdenite are also present. Key geological and geometrical characteristics of the Sungun copper mine (SCM) include a geological reserve of 796 Mt, a proven reserve of 410 Mt, an average grade of 0.67%, and a mine age of approximately 32 years. The overall stripping ratio is 1.7, with benches measuring 12.5 m in height, and slopes of 68° and 37° for the benches and overall pit, respectively. One of the undesirable outcomes of blasting operations at the Sungun mine is BB, with a maximum of 10 m recorded during previous operations. This issue prompted the authors to investigate BB more closely and develop a new method for its estimation. The primary explosive used at the mine is ANFO, with blasting cycles initiated by detonating cord. Stemming (St) material consists of drill cuttings, and the B–spacing (S) ratio varies across different parts of the deposit, depending on the specific characteristics of the blasting blocks. An image of BB following a blasting cycle is shown in Figure 3.

To compile a database for this study, 234 blasting operations were analyzed. Various factors, such as specific drilling (SD), hole length (HL), S, St, weight, powder factor (PF), and BB, were carefully considered. The methodology for measuring BB, as proposed by Bhatawdekar et al. [10], was employed in this study. BB was measured after each blast by first marking a reference line drawn 3 m parallel to the last row of blast holes. Following the blast, the extent of rock fracture behind this line was observed, and the perpendicular distance from the reference line to the fractured zone was recorded. This distance was taken as the BB value for each blast, following the procedure outlined by Bhatawdekar et al. [10].



FIGURE 2 | A view of Sungun copper mine [36].



FIGURE 3 | Back-break in the SCM after a blasting cycle [31].

Table 1 provides a statistical summary of the input parameters used to build the ML model. The variables include HL, B, S, St, SD, and PF, with the output variable being BB. The ranges for the input variables are as follows: HL (10–14 m), S (2–6.5 m), B (2–5 m), St(1.8–4.5 m), PD (0.2–0.93 kg/m^3), and SD (0.04–0.29 m). BB values range from 1 to 10 m Figure 4 illustrates the data distribution of these variables.

Figure 5 illustrates the linear relationships between the variables. The Pearson correlation coefficient (R, where $R \in (-1, 1)$) values are displayed within the boxes in the figure. A positive R value indicates a positive linear relationship between two variables, while a negative R value denotes a negative linear correlation. The closer the R value is to negative one, the stronger the negative correlation. As seen in Figure 5, BB shows significant correlations with HL, B, hole spacing, and St. These significant positive linear relationships are supported by their respective R values: 0.919 for HL, 0.939 for S, 0.945 for B, and 0.851 for St. In contrast, the PF and SD exhibit insignificant correlations.

3 | Methodology

3.1 | WOA

The WOA is an innovative optimization method introduced by Seyedali and Andrew [40]. This algorithm is based on the concept of swarm intelligence and is designed to mimic the hunting behavior of humpback whales, which involves locating prey, encircling it, pursuing it, and eventually attacking it. The fundamental concept behind WOA is straightforward, and its implementation requires adjusting only a few parameters,

3148, 2026, 1, Downloaded from https://onlinelibrary.wiley.com/doi/10.1155/vib/4973137 by National Health And Medical Research Council, Wiley Online Library on [18/11/2026]. See the Terms and Conditions (https://onlinelibrary.wiley.com/terms-and-conditions) on Wiley Online Library for rules of use; OA articles are governed by the applicable Creative Commons License

TABLE 1 | Statistical summary of 234 data samples.

Variable	Unit	Sort	Mean	Std. dev.	Median	Max	Min
B	m	Input	3.694	0.814	4	5	2
S	m	Input	4.528	0.899	4.5	6.5	2
PF	kg/m^3	Input	0.461	0.197	0.4	0.93	0.2
HL	m	Input	12.31	1.181	12.5	14	10
SD	m	Input	0.073	0.039	0.06	0.29	0.04
St	m	Input	3.664	0.762	4	4.5	1.8
BB	m	Output	4.321	2.542	4.0	10.0	1.0

making it relatively easy to program. According to Seyedali and Andrew [40], WOA offers superior accuracy and convergence speed compared to other optimization methods, such as gravitational search and particle swarm optimization (PSO) algorithms, particularly in optimizing objective functions.

Whales, the largest mammals on Earth, can grow up to 30 m in length and weigh as much as 180 tons. Their unique foraging behavior, known as bubble-net feeding [41], is illustrated in Figure 6. This feeding strategy involves two distinct phases: "upward spirals" and "double loops." In this process, the whale dives approximately 12 m below its prey and then spirals upward to create a bubble net, trapping the prey. The "double loops" maneuver includes the coral loop, lobtail loop, and capture loop [42].

The WOA is primarily inspired by this bubble-net feeding method. The algorithm considers a population of whales with a size of N and a search domain with a dimension of D. The position of the ith whale within the search domain is denoted as $(X_1^D, X_2^D, ..., X_N^D)$. The prey's position represents the global optimal solution for the problem. Since the global optimal position is initially unknown, the algorithm assumes that the current best position within the population is the prey. Consequently, all other whales in the population attempt to encircle the best individual. The current positions of the whales are updated using equation

$$X(t+1) = X_p(t) - A \times \left| C \times X_p(t) - X(t) \right|, \tag{1}$$

where t denotes the current iteration, $X_p(t)$ represents the prey's position, $X(t)$ represents the whales' positions, and A and C are coefficient vectors, derived from equations (2) and (3):

$$A = 2 \times \left(\frac{2-2t}{t_{\max}} \right) \times \text{rand}_1 - \left(\frac{2-2t}{t_{\max}} \right), \tag{2}$$

$$C = 2 \times \text{rand}_2. \tag{3}$$

Here, rand_1 and rand_2 are random values within the interval [0, 1], and $t_{\max}$ represents the maximum number of iterations.

The WOA employs two distinct approaches to mathematically simulate the bubble-net feeding behavior of whales: the shrinking encircling mechanism (equation (2)) and the spiral updating location mechanism, which models the spiral motion of the whale as described in the following equation:

$$X(t+1) = \overrightarrow{D'} \times e^{bl} \times \cos(2\pi l) + X_p(t), \tag{4}$$

where D' represents the distance between the ith whale and the prey, b is a constant that controls the shape of the logarithmic spiral, and l is a random value within the interval $[-1, 1]$. During optimization, it is important to consider the probability of the WOA selecting the updating location, which in this study has been set to 0.5.

In addition to bubble-net feeding behavior, whales can also engage in random search behavior, where individual whales perform searches based on the positions of other whales. This behavior is mathematically represented by equation (5):

$$X(t+1) = X_{\text{rand}}(t) - A \times \left| C \times X_{\text{rand}}(t) - X(t) \right|, \tag{5}$$

where $X_{\text{rand}}(t)$ represents the position of a whale randomly selected from the current iteration.

The flowchart of the WOA is depicted in Figure 7.

3.2 | Justification for Selecting WOA

The WOA was chosen over other metaheuristic techniques such as genetic algorithm (GA), PSO, and Bayesian optimization due to several advantages relevant to this study. First, WOA requires fewer control parameters, which simplifies implementation and reduces the risk of parameter tuning errors. Second, WOA has demonstrated faster convergence and superior accuracy in high-dimensional optimization problems compared with GA and PSO, as reported by Yari and Andrew (2016). Third, prior studies in mining and geotechnical engineering have successfully applied WOA for optimizing ML models, confirming its robustness and reliability in similar contexts (Yari et al., 2023). While Bayesian optimization is a powerful probabilistic approach, it typically demands higher computational resources and complex modeling, which was beyond the scope of this work. These factors collectively make WOA an efficient and practical choice for hyperparameter optimization in the LightGBM model.

3.3 | LightGBM

LightGBM is an advanced version of the gradient boosting decision tree (GBDT) method, designed to handle large, high-dimensional datasets with enhanced training speed and accuracy [43]. It is known for its efficient memory usage and support for distributed parallel computing, enabling the rapid processing of vast amounts of data. The following are the key characteristics of LightGBM:

- Leaf-wise tree growth strategy: unlike the conventional GBDT algorithm, which grows trees level-wise, LightGBM

3148, 2026, 1, Downloaded from https://onlinelibrary.wiley.com/doi/10.1155/vib/4973137 by National Health And Medical Research Council, Wiley Online Library on [18/11/2026]. See the Terms and Conditions (https://onlinelibrary.wiley.com/terms-and-conditions) on Wiley Online Library for rules of use; OA articles are governed by the applicable Creative Commons License

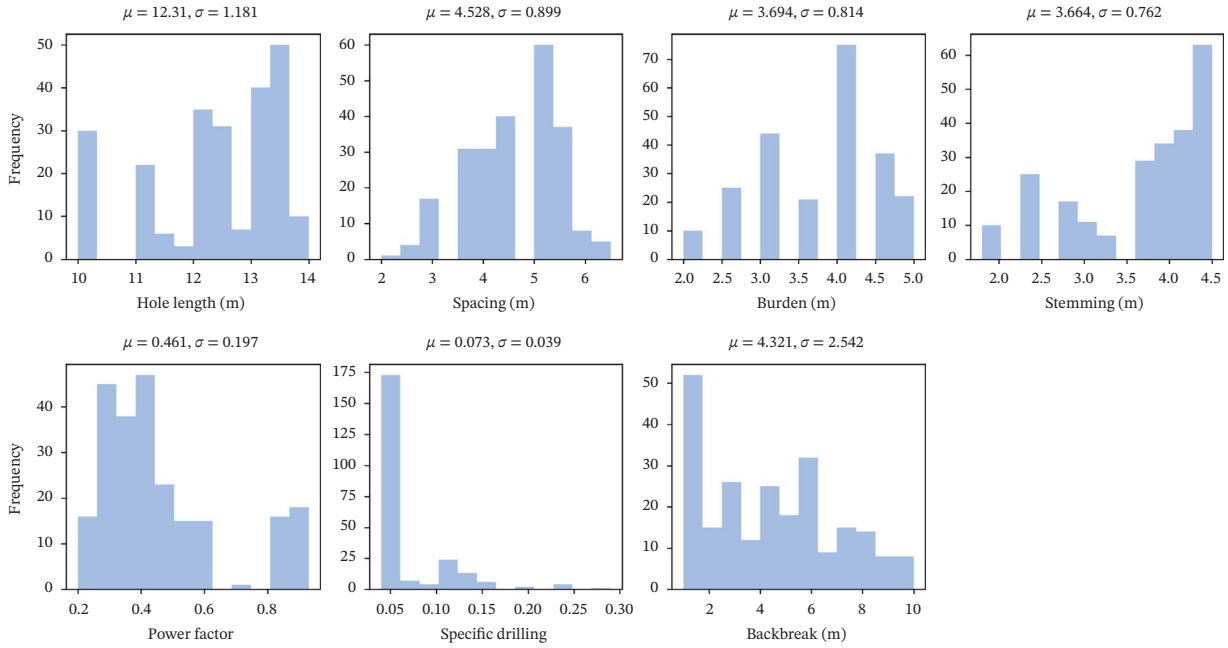


FIGURE 4 | Histogram of the variables (μ is mean and σ is std. dev.).

employs a leaf-wise tree growth strategy with constraints on maximum depth. This approach involves splitting only the leaf node with the highest information gain during each traversal of all current leaf nodes. Consequently, the leaf-wise strategy results in lower error and higher efficiency compared to the traditional GBDT algorithm, given the same number of splits [44]. To prevent overfitting, LightGBM also limits the maximum depth of the decision tree.

- Histogram algorithm: LightGBM utilizes a histogram algorithm to process features. This method discretizes features into K integers, creating a histogram with K bins. As data samples are traversed, the histogram accumulates statistics, which are then used to identify the best splitting nodes based on the discrete feature statistics [45]. This process reduces the time and memory required for selecting splitting nodes, making it suitable for datasets with large volumes of data and high dimensionality.



FIGURE 5 | Correlation heatmap of the variables.

3148, 2026, 1, Downloaded from https://onlinelibrary.wiley.com/doi/10.1155/vib/4973137 by National Health And Medical Research Council, Wiley Online Library on [18/11/2026]. See the Terms and Conditions (https://onlinelibrary.wiley.com/terms-and-conditions) on Wiley Online Library for rules of use; OA articles are governed by the applicable Creative Commons License

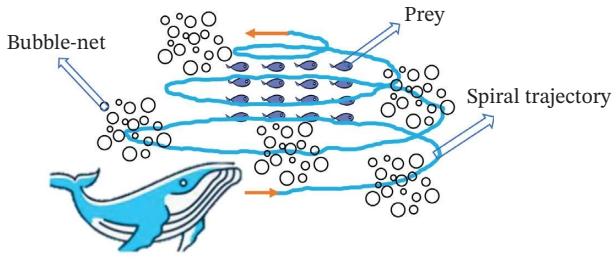


FIGURE 6 | Feeding behavior of whales.

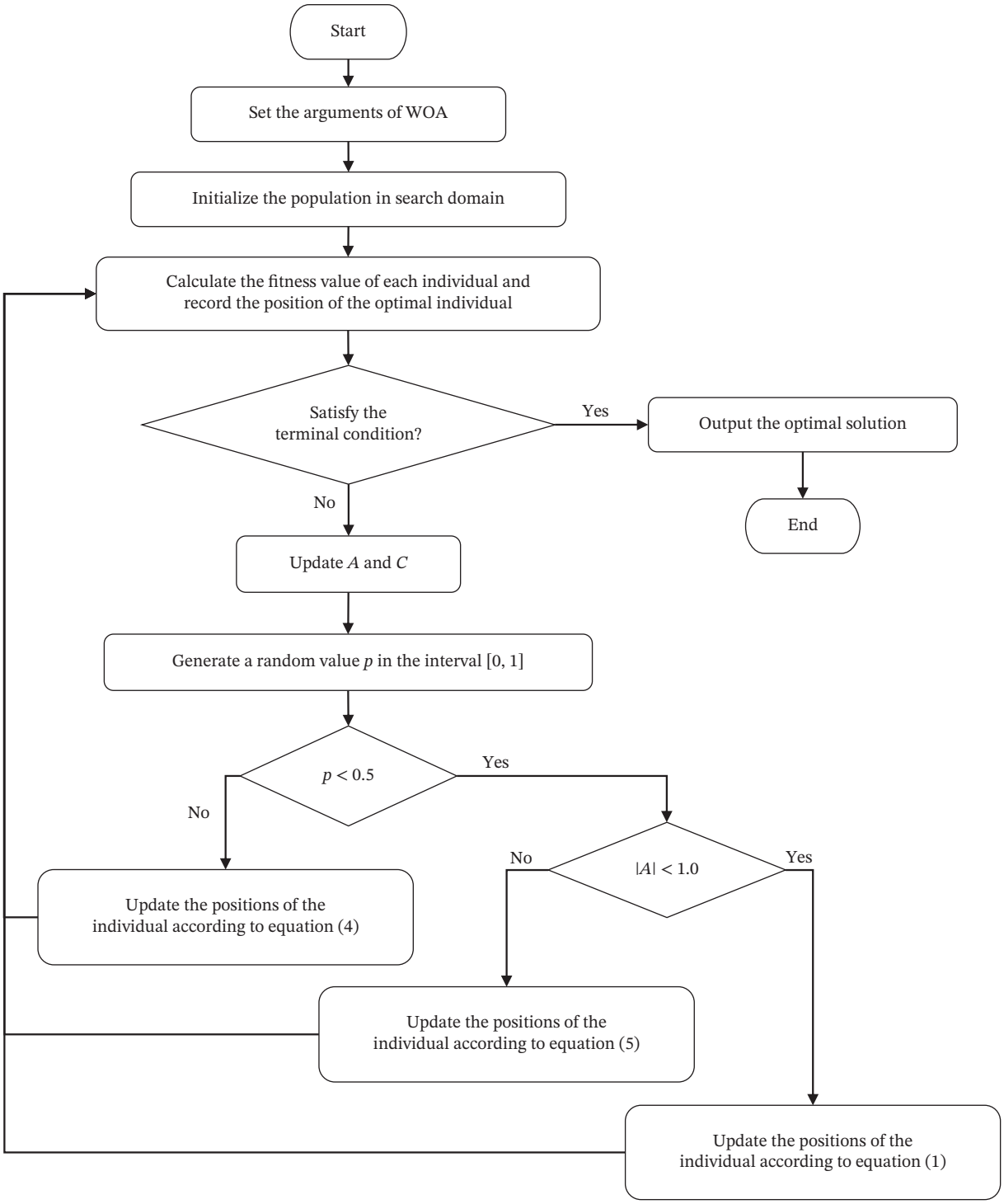


FIGURE 7 | Flowchart of WOA.

3148, 2026, 1, Downloaded from https://onlinelibrary.wiley.com/doi/10.1155/vib/4973137 by National Health And Medical Research Council, Wiley Online Library on [18/11/2026]. See the Terms and Conditions (https://onlinelibrary.wiley.com/terms-and-conditions) on Wiley Online Library for rules of use; OA articles are governed by the applicable Creative Commons License

- Gradient-based one-side sampling (GOSS): to enhance training efficiency, LightGBM introduces the GOSS algorithm, which reduces the amount of data used for training. The algorithm sorts the training data based on gradient values and divides the samples into high-gradient and low-gradient categories. All high-gradient samples are retained, while a random percentage of low-gradient samples is selected. An amplification factor is applied to the retained low-gradient samples to ensure that this process does not distort the original sample distribution. This way, LightGBM focuses more on high-gradient samples when calculating information gain.
- Exclusive feature bundling (EFB): unlike the GOSS algorithm, the EFB algorithm improves model training speed by optimizing feature extraction. Traditional feature extraction reduces the dimensionality of training data by eliminating irrelevant features. In contrast, the EFB method reduces feature dimensionality by bundling mutually exclusive features together. In high-dimensional data, some features in the sparse feature space are mutually exclusive, meaning they are unlikely to be nonzero simultaneously. By bundling these incompatible features into a single feature package, computational effort is significantly reduced. The structure of WOA is depicted in Figure 8.

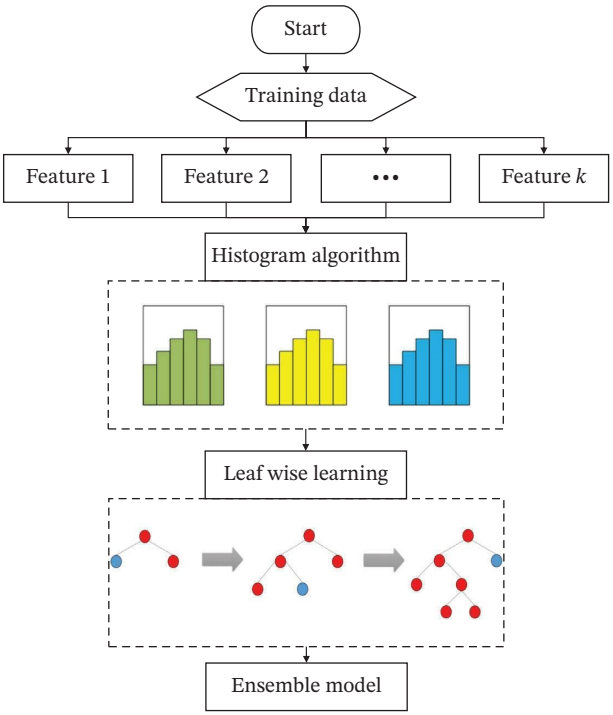


FIGURE 8 | Structure of the LightGBM model.

3.4 | Optimized LightGBM-Based Models

The performance of ML models, including LightGBM, heavily depends on the selection of hyperparameters, with different combinations yielding varying results. The LightGBM model includes numerous hyperparameters, and optimizing these is crucial to achieving the best possible performance. In this study, the WOA was used to optimize the hyperparameters of the LightGBM model.

Before building the hybrid WOA–LightGBM model, the dataset, comprising 234 samples, was randomly split into two parts: 80% (188 samples) for training and 20% (46 samples) for model evaluation. It is important to note that prior to the model process, the dataset was checked for missing values, cleaned, and normalized to ensure consistency across input variables. The WOA was then used to find the optimal hyperparameter values. The main steps for training the hybrid WOA–LightGBM model are as follows:

- Determine the range of hyperparameters: the LightGBM model was established with hyperparameters including n_estimators, learning_rate, and subsample. In this study, n_estimators, the number of boosting iterations, was set to 100. The learning_rate and subsample, which represent the learning rate and subsample ratio of the training data, respectively, needed to be optimized using WOA. The boundaries for learning_rate and subsample were set to [0.01, 0.30] and [0.2, 0.8], respectively.
- Define the objective function: WOA, designed for solving minimization problems, was used to optimize the LightGBM model by minimizing the RMSE. The RMSE measures the difference between the actual values and those predicted by the LightGBM model. By minimizing RMSE, WOA identifies the optimal values for hyperparameters like the learning rate and subsample. Additionally, a 5-fold cross-validation method was employed to enhance the model's robustness and reliability.
- Optimize the hyperparameters: during the WOA's hyperparameter search, the next set of hyperparameters is chosen based on the minimization of the RMSE value throughout the optimization process. Iteration results, including each hyperparameter set and corresponding RMSE values, are recorded. The loop continues until the specified number of iterations is completed, at which point the optimal hyperparameter values are determined. In this study, the WOA was configured to run for 200 iterations with a population size of 150.

It is worth noting that hybrid tree-based techniques, combined with one or more optimization algorithms, have been successfully applied in various civil and mining engineering tasks, including tunnel construction [46, 47], slope stability [48, 49], mechanical behavior of rock samples [50, 51], and blasting operations [9, 52].

4 | Results and Discussion

4.1 | Modeling Results

This section presents and discusses the process of developing an ML model to predict blast-induced BB, specifically focusing on the training phase of the WOA–LightGBM model. It is important to mention that the authors have tried other tree-based models, i.e., RF and XGBoost, together with LightGBM, in order to check their prediction performance. As a result, the prediction capacity of LightGBM was slightly higher than other applied techniques, and because of that, the authors decided to continue the modeling process with LightGBM.

Figure 9 illustrates the training iteration results of the proposed approach. The WOA–LightGBM model did not achieve convergence until around the 10th iteration. After this point, the fitness value remained stable, with no further changes observed.

3148, 2026, 1, Downloaded from https://onlinelibrary.wiley.com/doi/10.1155/vib/4973137 by National Health And Medical Research Council, Wiley Online Library on [18/11/2026]. See the Terms and Conditions (https://onlinelibrary.wiley.com/terms-and-conditions) on Wiley Online Library for rules of use; OA articles are governed by the applicable Creative Commons License

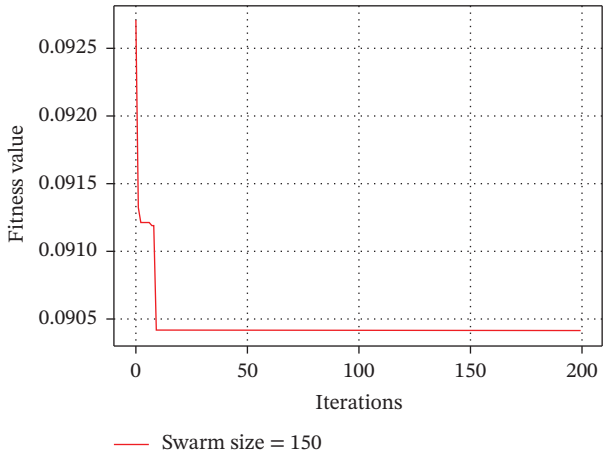


FIGURE 9 | Iteration results of the WOA–LightGBM model.

By the time the model reached 200 iterations, the WOA had determined the optimal values for the two hyperparameters of the LightGBM model, resulting in a learning rate of 0.252 and a subsample ratio of 0.28.

Figure 10 provides a three-dimensional representation of alternative solutions to visually depict the optimal solution within the domain space. The bottom two axes represent the learning rate and subsample, while the vertical axis corresponds to the fitness values. The red point highlights the best solutions for the learning rate and subsample, which are 0.252 and 0.28, respectively. The remaining colored points indicate the fitness values calculated for learning rates within the [0.01, 0.30] interval and subsample ratios within the [0.2, 0.8] interval. Intuitively, the optimal solution for the WOA–LightGBM model appears to involve a high learning rate combined with a low subsample ratio.

4.2 | Model Evaluation

After completing the model training and identifying the optimal hyperparameters, the next step involves evaluating the model's performance. This evaluation utilizes five metrics: R^2, variance

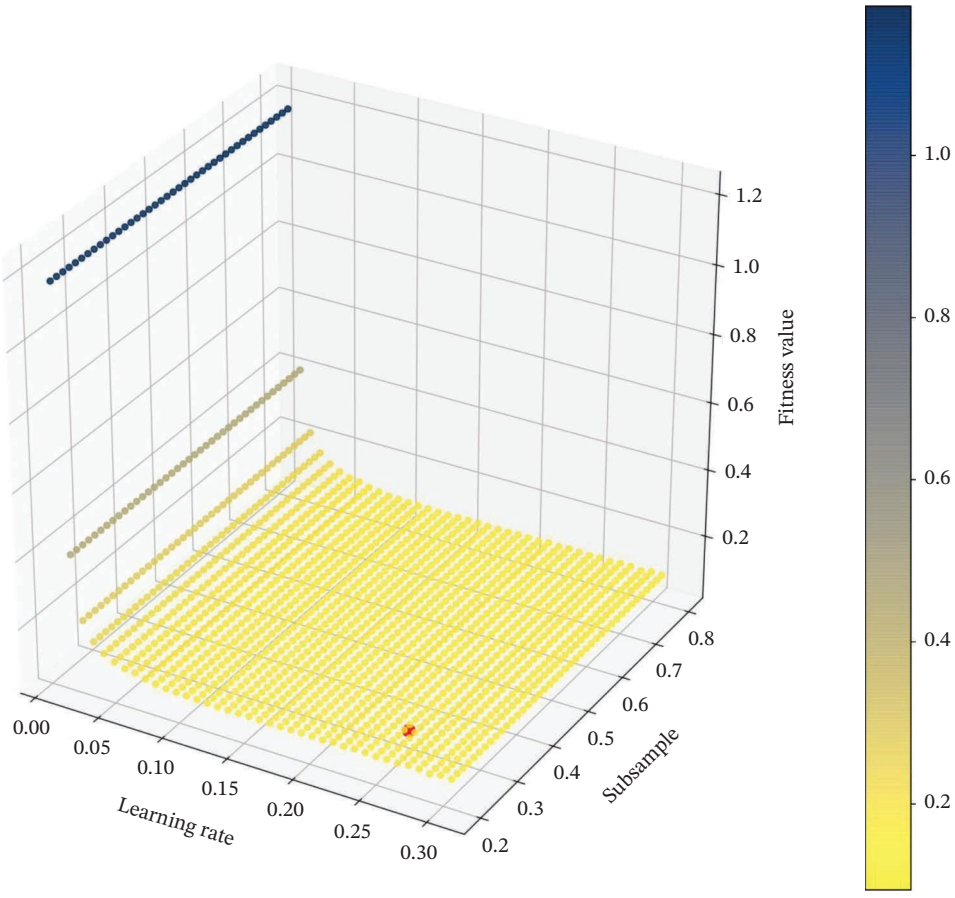


FIGURE 10 | Optimal solution for the WOA–LightGBM model in the solution space.

3148, 2026, 1, Downloaded from https://onlinelibrary.wiley.com/doi/10.1155/vib/4973137 by National Health And Medical Research Council, Wiley Online Library on [18/11/2026]. See the Terms and Conditions (https://onlinelibrary.wiley.com/terms-and-conditions) on Wiley Online Library for rules of use; OA articles are governed by the applicable Creative Commons License

accounted for (VAF), mean absolute error (MAE), RMSE, and mean absolute percentage error (MAPE). These metrics are commonly used in regression tasks to gauge the accuracy of trained models. The following formulas are used to calculate these metrics:

$$R^2 = 1 - \frac{\sum_{i=1}^{n}(y_i - \hat{y}_i)^2}{\sum_{i=1}^{n}(y_i - \bar{y})^2}, \tag{6}$$

$$\mathrm{VAF} = \left(1 - \frac{\mathrm{var}(y_i - \hat{y}_i)}{\mathrm{var}(y_i)}\right) \times 100\%, \tag{7}$$

$$\mathrm{RMSE} = \sqrt{\frac{1}{n}\sum_{i=1}^{n}(y_i - \hat{y}_i)^2}, \tag{8}$$

$$\mathrm{MAE} = \frac{1}{n}\sum_{i=1}^{n}|y_i - \hat{y}_i|, \tag{9}$$

$$\mathrm{MAPE} = \frac{1}{n}\sum_{i=1}^{n}\left|\frac{y_i - \hat{y}_i}{y_i}\right|, \tag{10}$$

where y_i, $\hat{y}_i$, and $\bar{y}$ represent the true, predicted, and mean values of the target variable (BB in this study), respectively, and n represents the number of data samples. An ideal ML model would have an R^2 value close to 1, a VAF close to 100%, and RMSE, MAE, and MAPE values close to 0.

On the training set, the WOA–LightGBM model achieves the following performance metrics: an R^2 of 0.997, a VAF of 99.651%, an RMSE of 0.152, an MAE of 0.098, and a MAPE of 0.022. When applied to the testing set, the model achieves an R^2 of 0.990, a VAF of 99.030%, an RMSE of 0.230, an MAE of 0.132, and a MAPE of 0.032. These results indicate that the WOA–LightGBM model is highly accurate in predicting blast-induced BB. Additionally, the results for the training set are slightly better than those for the testing set. Figure 11 visually compares the predicted BB values from the WOA–LightGBM model with the actual measured values, showing that most predicted results

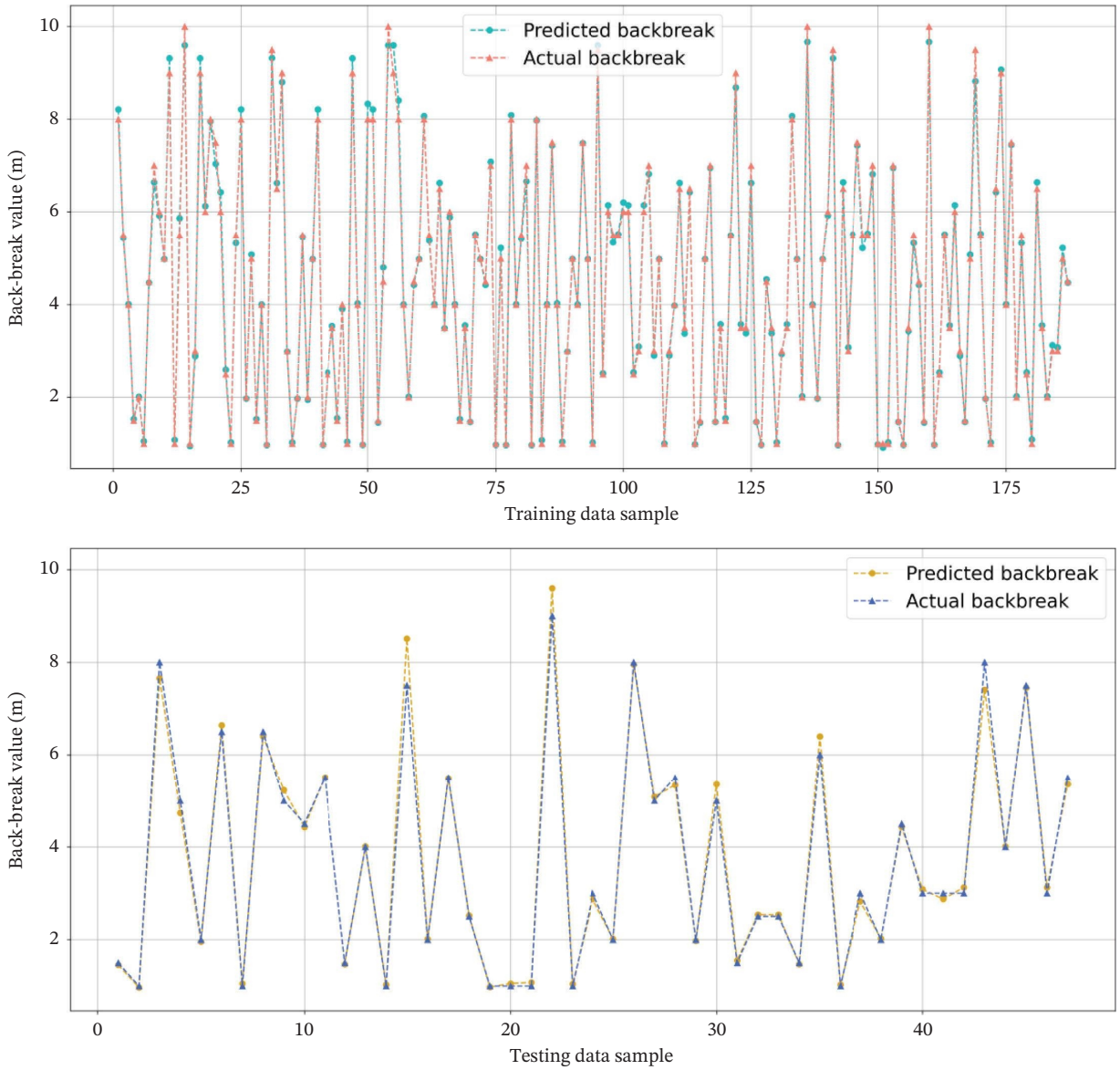


FIGURE 11 | Back-break values (predicted and measured) for the training set.

3148, 2026, 1, Downloaded from https://onlinelibrary.wiley.com/doi/10.1155/vib/4973137 by National Health And Medical Research Council, Wiley Online Library on [18/11/2026]. See the Terms and Conditions (https://onlinelibrary.wiley.com/terms-and-conditions) on Wiley Online Library for rules of use; OA articles are governed by the applicable Creative Commons License

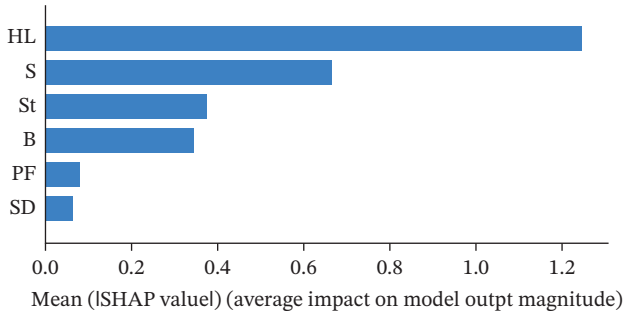


FIGURE 12 | Feature contribution (|SHAP value|).

closely match the actual BB, further confirming the model's strong predictive performance.

4.3 | Sensitivity Analysis

Accurately predicting BB is crucial in mining blasting operations, as it significantly reduces the risks of rock loosening and collapse. Since BB occurrence is influenced by factors like blasting design elements and explosive material properties, it is essential to investigate how these factors specifically affect BB in this project. To achieve this, the SHAP methodology was used to evaluate the results produced by the WOA–LightGBM model and to quantify the contributions of individual components. The SHAP method allows for the determination of the importance of specific features by analyzing the mean magnitude of SHAP values [9, 44]. Additionally, SHAP provides a visualization of how individual features impact the model's outputs. In this study, the tree explainer of SHAP was utilized to explain the influence of each feature on the outputs generated by the WOA–LightGBM model.

As depicted in Figure 12, it is evident that HL has the most significant influence on the model output (i.e., BB), with S being about half as influential as HL. This is followed by St and B, which contribute less to the model output compared with HL and S. The impact of PF and SD on the model output is negligible.

While Figure 12 provides an overview of the relative importance of each input in the model, it does not convey the specific impact of each feature on BB development. To address this, the SHAP summary plot was employed. As shown in Figure 13, each point on the plot represents the SHAP value of an instance, corresponding to a specific feature. The *y*-axis lists the feature categories, while the *x*-axis represents the SHAP values of individual features. Higher feature values are indicated in red, whereas lower values are shown in blue. The color of the points reflects the feature value. By using the SHAP summary plot, a more detailed understanding of how individual features influence BB development can be obtained.

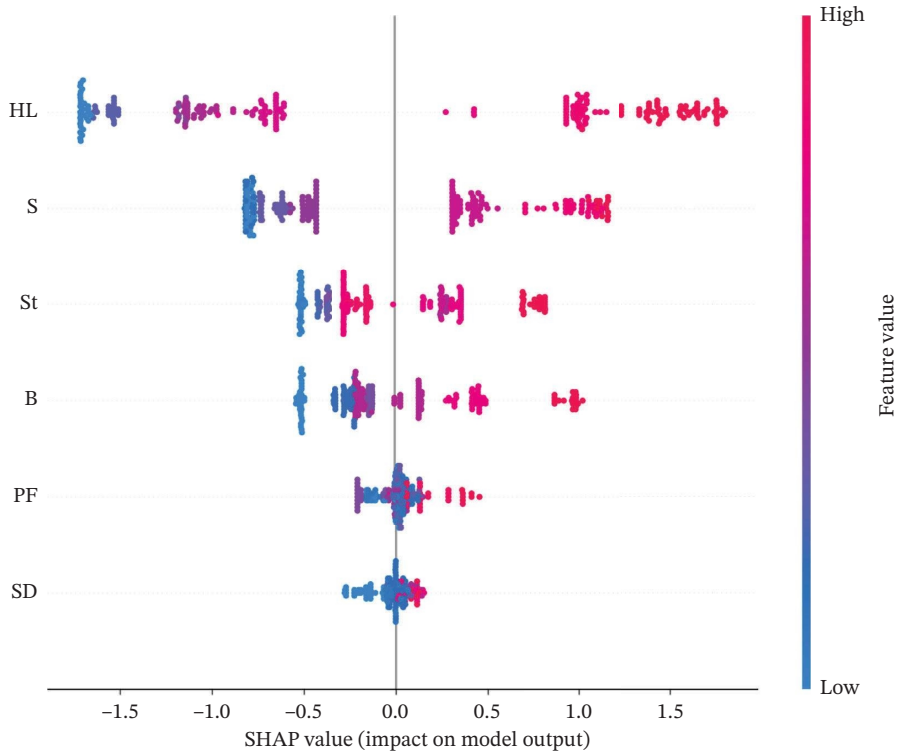


FIGURE 13 | SHAP summary plot for the features used.

3148, 2026, 1, Downloaded from https://onlinelibrary.wiley.com/doi/10.1155/vib/4973137 by National Health And Medical Research Council, Wiley Online Library on [18/11/2026]. See the Terms and Conditions (https://onlinelibrary.wiley.com/terms-and-conditions) on Wiley Online Library for rules of use; OA articles are governed by the applicable Creative Commons License

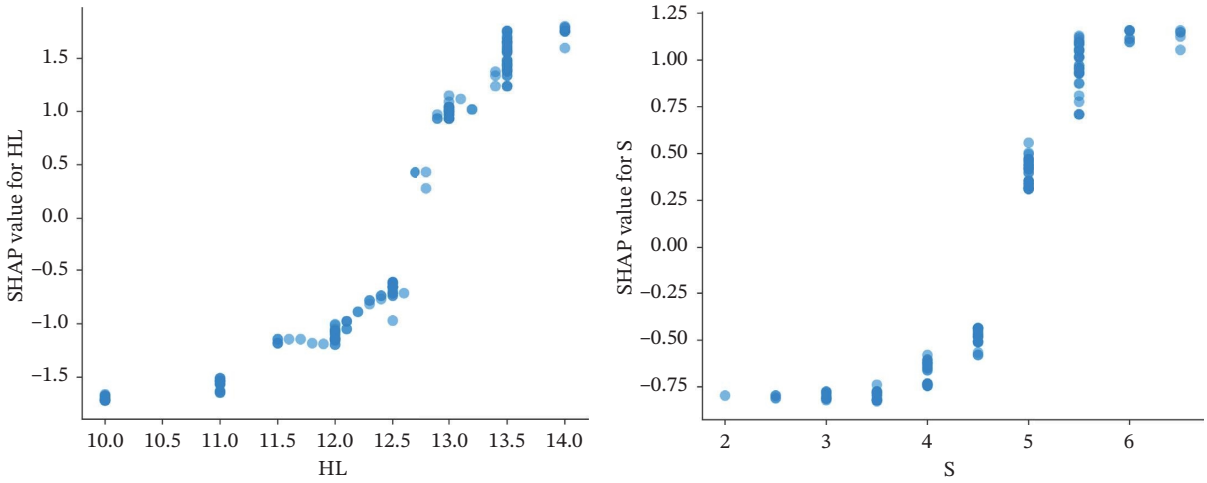


FIGURE 14 | The influence of HL and S on back-break based on SHAP calculations.

For example, examining HL reveals that higher SHAP values correspond to higher HL values, indicating that the likelihood of BB increases as HL increases. Conversely, lower HL values are associated with lower SHAP values, suggesting that minimizing HL can help reduce BB development. The influence pattern of S on BB development is similar to that of HL, albeit slightly less pronounced. In contrast, St and B exhibit the same influence pattern as HL and S, but their impact is much lower. Regarding PF and SD, their SHAP values are concentrated around zero, implying that their influence on BB development is minimal.

The SHAP results reveal that longer HL and wider S significantly increase the likelihood of BB, as they promote greater crack propagation behind the final row. St and B also influence BB but to a lesser degree, mainly through their effects on energy confinement. These insights highlight how small adjustments in key blasting parameters can substantially affect BB, offering practical guidance for optimizing blast design.

Given that HL and S significantly affect BB occurrence, the discussion will now focus on how HL and S contribute to this phenomenon. Figure 14 shows that the risk of BB is low when the HL value is between 10.0 and 12.5 m but increases gradually as HL values rise from 13.0 to 14.0 m. Similarly, for S, the risk of BB is low when its value is below 4.5 m but increases progressively when it exceeds 5.0 m. These findings suggest that BB can be effectively managed by adjusting the length of blast holes and the S between them.

5 | Limitations and Future Studies

This study introduced a model for predicting BB, trained on a database comprising 234 blasting operations. While this is a relatively large dataset compared with existing studies, where fewer than 100 operations were often analyzed, the database can still be expanded in several ways. One approach is to increase the number of effective (input) parameters, whether related to the blasting pattern or geological conditions. Another approach involves broadening the range of each variable (input or output) in the database, which would allow for the development of a more general ML model that can address a wider range of scenarios within the same problem domain.

Additionally, this study utilized only one optimization algorithm, the WOA, to determine the hyperparameters of the LightGBM model. Future research could explore the potential of other optimization algorithms, such as the tunicate swarm algorithm or the sparrow search algorithm, in conjunction with the same base model (LightGBM). Furthermore, alternative base models from the same family as LightGBM, such as Adaptive Boosting Machine or Extreme Gradient Boosting, could be employed by other researchers to evaluate their effectiveness in predicting blast-induced BB.

5.1 | Generalization and Industrial Adoption

Although the proposed WOA–LightGBM model achieved high predictive accuracy using data from the Sungun mine, its generalization to other geological and operational settings requires further validation. Future research should incorporate multisite datasets encompassing diverse rock types, blasting patterns, and environmental conditions to ensure model robustness. For industrial adoption, the following steps are recommended: (1) integration with blast design software to enable real-time prediction and optimization of BB. (2) Continuous retraining of the model using site-specific data to maintain accuracy under varying conditions. (3) Pilot testing in collaboration with mining companies to evaluate practical feasibility and operational benefits. The adaptability of LightGBM to heterogeneous datasets supports its scalability, but comprehensive benchmarking across different mines is essential before large-scale implementation.

6 | Conclusions

The study successfully applied the WOA to identify the optimal hyperparameters for the LightGBM model, resulting in a learning rate of 0.252 and a subsample value of 0.28. The performance of the developed WOA–LightGBM model was rigorously evaluated using five key metrics: the R^2, VAF, RMSE, MAE, and MAPE. The model demonstrated outstanding predictive accuracy, achieving an R^2 of 0.997, a VAF of 99.651%, and an RMSE of 0.152 on the training dataset. On the testing dataset, the model maintained strong performance, with an R^2 of 0.990, a VAF of 99.030%, and an RMSE of 0.230. These results underscore the robustness and reliability of the WOA–LightGBM model in predicting BB, a critical factor in mining and blasting operations.

3148, 2026, 1, Downloaded from https://onlinelibrary.wiley.com/doi/10.1155/vib/4973137 by National Health And Medical Research Council, Wiley Online Library on [18/11/2026]. See the Terms and Conditions (https://onlinelibrary.wiley.com/terms-and-conditions) on Wiley Online Library for rules of use; OA articles are governed by the applicable Creative Commons License

In addition to the model's performance metrics, the study employed the SHAP method, which provides an interpretable approach for understanding the contributions of individual features in tree-based ML models. Through SHAP analysis, it was revealed that certain input variables, specifically HL and S, exert a significant influence on the development of BB in the studied engineering scenario. The SHAP dependence plots provided valuable insights into how variations in these features affect the model's output, highlighting that reducing the length of blast holes and minimizing the S between them are effective strategies for mitigating BB risk. The implications of these findings are particularly relevant for the field of mining engineering, where the precise control of blasting parameters is essential for minimizing operational risks and optimizing outcomes. By maintaining borehole depths below 12.5 m and ensuring S is less than 4.5 m, it is possible to significantly reduce the likelihood of BB occurrences, thereby improving the safety and efficiency of blasting operations. The success of the SHAP analysis in this context highlights the value of interpretable ML techniques in engineering applications, offering a clear understanding of model behavior and contributing to more informed decision-making processes.

The contribution of this study is not only proposing a ML model (i.e., the WOA–LightGBM) with a high degree of accuracy in predicting BB resulting from blasting but also introducing a practical way that can be used by mining engineers and designers. The model with its input parameters and specifications could be used in similar cases where they have had such problems before the operation and based on the historical data. It will help to at least give some better and clearer view to the designers regarding the possible results of BB after the operations.

Nomenclature

WOA	Whale optimization algorithm
LightGBM	Light gradient boosting machine
SHAP	Shapley additive explanations
VAF	Variance accounted for
R^2	Coefficient of determination
RMSE	Root mean square error
MAE	Mean absolute error
MAPE	Mean absolute percentage error
GBDT	Gradient boosting decision tree
GOSS	Gradient-based one-side sampling
EFB	Exclusive feature bundling
ML	Machine learning
SD	Specific drilling
PF	Powder factor
HL	Hole length
B	Burden
S	Spacing
St	Stemming
BB	Back-Break

Author Contributions

Conceptualization: Mojtaba Yari, Danial Jahed Armaghani, Manoj Khandelwal, Hadi Fattahi, and Xuzhen He. Methodology: Biao He, Mojtaba Yari, and Danial Jahed Armaghani. Software: Biao He and Mojtaba Yari. Validation: Biao He, Danial Jahed Armaghani, and Payam Abbasi. Data curation: Mojtaba Yari. Writing the original draft: Mojtaba Yari, Biao He, Payam Abbasi, Danial Jahed Armaghani, Manoj Khandelwal, Hadi Fattahi, and Xuzhen He. Writing–review and editing: Mojtaba Yari, Biao He, Payam Abbasi, Danial Jahed Armaghani, Manoj Khandelwal, Hadi Fattahi, and Xuzhen He. Supervision: Danial Jahed Armaghani, Manoj Khandelwal, and Hadi Fattahi.

Acknowledgments

The authors wish to appreciate the Sungun mine and its manager, who helped much during the data collection of this study.

Funding

No funding was received for this manuscript.

Conflicts of Interest

The authors declare no conflicts of interest.

Data Availability Statement

Data will be made available on request from the corresponding author.

References

1. H. L. Hartman and J. M. Mutmansky, *Introductory Mining Engineering* (John Wiley & Sons, 2002).

2. H. Jang, Y. Kawamura, and U. Shinji, "An Empirical Approach of Overbreak Resistance Factor for Tunnel Blasting," *Tunnelling and Underground Space Technology* 92 (2019): 103060, https://doi.org/10.1016/j.tust.2019.103060.

3. M. Khandelwal and T. N. Singh, "Prediction of Blast-Induced Ground Vibration Using Artificial Neural Network," *International Journal of Rock Mechanics and Mining Sciences* 46, no. 7 (2009): 1214–1222, https://doi.org/10.1016/j.ijrmms.2009.03.004.

4. M. Khandelwal, "Evaluation and Prediction of blast-Induced Ground Vibration Using Support Vector Machine," *International Journal of Rock Mechanics and Mining Sciences* 47, no. 3 (2010): 509–516, https://doi.org/10.1016/j.ijrmms.2010.01.007.

5. M. Saadat, M. Khandelwal, and M. Monjezi, "An ANN-Based Approach to Predict Blast-Induced Ground Vibration of Gol-E-Gohar Iron Ore Mine, Iran," *Journal of Rock Mechanics and Geotechnical Engineering* 6, no. 1 (2014): 67–76, https://doi.org/10.1016/j.jrmge.2013.11.001.

6. N. K. Dumakor-Dupey, S. Arya, and A. Jha, "Advances in blast-induced Impact prediction—A Review of Machine Learning Applications," *Minerals* 11, no. 6 (2021): 601, https://doi.org/10.3390/min11060601.

7. M. Khandelwal and M. Monjezi, "Prediction of Backbreak in open-pit Blasting Operations Using the Machine Learning Method," *Rock Mechanics and Rock Engineering* 46, no. 2 (2013): 389–396, https://doi.org/10.1007/s00603-012-0269-3.

8. C. J. Konya and E. J. Walter, *Rock Blasting and Overbreak Control* (United States: Federal Highway Administration, 1991).

9. M. Yari, B. He, D. J. Armaghani, P. Abbasi, and E. T. Mohamad, "A Novel Ensemble Machine Learning Model to Predict Mine blasting–induced Rock Fragmentation," *Bulletin of Engineering Geology and the Environment* 82, no. 5 (2023): 187, https://doi.org/10.1007/s10064-023-03138-y.

10. S. Behera and K. Dey, "Prediction of Backbreak in Surface Production Blasting Using 3-Dimensional Finite Element Modeling and 3-Dimensional Nearfield Vibration Modeling," *Mining, Metallurgy &*

3148, 2026, 1, Downloaded from https://onlinelibrary.wiley.com/doi/10.1155/vib/4973137 by National Health And Medical Research Council, Wiley Online Library on [18/11/2026]. See the Terms and Conditions (https://onlinelibrary.wiley.com/terms-and-conditions) on Wiley Online Library for rules of use; OA articles are governed by the applicable Creative Commons License

Exploration 41, no. 6 (2024): 3147–3162, https://doi.org/10.1007/s42461-024-01072-5.

11. M. Monjezi and H. Dehghani, "Evaluation of Effect of Blasting Pattern Parameters on Back Break Using Neural Networks," *International Journal of Rock Mechanics and Mining Sciences* 45, no. 8 (2008): 1446–1453, https://doi.org/10.1016/j.ijrmms.2008.02.007.

12. D. C. Wyllie and C. W. Mah, "Wedge Failure," in *Rock Slope Engineering* (CRC Press, 2017), 153–175.

13. N. Lundborg, "The Hazards of Flyrock in Rock Blasting," *Reports DS* 12 (1974).

14. J. Roth, "A Model for the Determination of Flyrock Range as a Function of Shot Conditions," *NTIS* (1979).

15. A. Sayadi, M. Monjezi, N. Talebi, and M. Khandelwal, "A Comparative Study on the Application of Various Artificial Neural Networks to Simultaneous Prediction of Rock Fragmentation and Backbreak," *Journal of Rock Mechanics and Geotechnical Engineering* 5, no. 4 (2013): 318–324, https://doi.org/10.1016/j.jrmge.2013.05.007.

16. M. Sharma, H. Agrawal, and B. Choudhary, "Multivariate Regression and Genetic Programming for Prediction of Backbreak in open-pit Blasting," *Neural Computing & Applications* 34, no. 3 (2022): 1–12, https://doi.org/10.1007/s00521-021-06553-y.

17. M. Esmaeili, M. Osanloo, F. Rashidinejad, A. Aghajani Bazzazi, and M. Taji, "Multiple Regression, ANN and ANFIS Models for Prediction of Backbreak in the Open Pit Blasting," *Engineering With Computers* 30, no. 4 (2014): 549–558, https://doi.org/10.1007/s00366-012-0298-2.

18. M. Sari, E. Ghasemi, and M. Ataei, "Stochastic Modeling Approach for the Evaluation of Backbreak due to Blasting Operations in Open Pit Mines," *Rock Mechanics and Rock Engineering* 47, no. 2 (2014): 771–783, https://doi.org/10.1007/s00603-013-0438-z.

19. A. K. Sirjani, F. Sereshki, M. Ataei, and M. A. Hosseini, "Prediction of Backbreak in the Blasting Operations Using Artificial Neural Network (ANN) Model and Statistical Models (Case Study: Gol-E-Gohar Iron Ore Mine No. 1)," *Archives of Mining Sciences* (2022).

20. A. A. Bazzazi and M. Esmaeili, "Prediction of Backbreak in Open Pit Blasting by Adaptive neuro-fuzzy Inference System," *Archives of Mining Sciences* 57, no. 4 (2012).

21. H. Naderpour and M. Mirrashid, "A Neuro-Fuzzy Model for Punching Shear Prediction of slab-column Connections Reinforced with FRP," *Journal of Soft Computing in Civil Engineering* 3, no. 1 (2019): 16–26.

22. Z. Yu, X. Shi, J. Zhou, et al., "Feasibility of the Indirect Determination of blast-induced Rock Movement Based on Three New Hybrid Intelligent Models," *Engineering With Computers* 37, no. 2 (2021): 991–1006, https://doi.org/10.1007/s00366-019-00868-0.

23. X. Ye, H. Moayedi, M. Khari, and L. K. Foong, "Metaheuristic-Hybridized Multilayer Perceptron in Slope Stability Analysis," *Smart Structures and Systems, An International Journal* 26, no. 3 (2020): 263–275.

24. C. Y. Huat, D. J. Armaghani, S. H. Lai, H. Motaghedi, P. G. Asteris, and P. Fakharian, "Analyzing Surface Settlement Factors in Single and Twin Tunnels: a Review Study," *Journal of Engineering Research* 13, no. 3 (2024): 2096–2108, https://doi.org/10.1016/j.jer.2024.05.009.

25. A. Ziaie, B. Mehdizadeh, F. Safi Jahanshahi, N. Ahmadi, and A. R. Ghanizadeh, "Prediction of Liquefaction-Induced Lateral Displacements Using Hybrid GBRT and EOA," *Journal of Soft Computing in Civil Engineering* 10, no. 1 (2026): e225827.

26. D. J. Armaghani, E. T. Mohamad, M. S. Narayanasamy, N. Narita, and S. Yagiz, "Development of Hybrid Intelligent Models for Predicting TBM Penetration Rate in Hard Rock Condition," *Tunnelling and Underground Space Technology* 63 (2017): 29–43, https://doi.org/10.1016/j.tust.2016.12.009.

27. P. G. Asteris, M. Karoglou, A. D. Skentou, et al., "Predicting Uniaxial Compressive Strength of Rocks Using ANN Models: Incorporating Porosity, Compressional Wave Velocity, and Schmidt Hammer Data," *Ultrasonics* 141 (2024): 107347, https://doi.org/10.1016/j.ultras.2024.107347.

28. P. Nobahar, R. Shirani Faradonbeh, S. N. Almasi, and R. Bastami, "Advanced AI-powered Solutions for Predicting blast-induced Flyrock, Backbreak, and Rock Fragmentation," *Mining, Metallurgy & Exploration* 41, no. 4 (2024): 2099–2118, https://doi.org/10.1007/s42461-024-01028-9.

29. P. Ragam, A. R. Komalla, and N. Kanne, "Estimation of blast-induced Peak Particle Velocity Using Ensemble Machine Learning Algorithms: a Case Study," *Noise & Vibration Worldwide* 53, no. 7-8 (2022): 404–413, https://doi.org/10.1177/09574565221114662.

30. N. M. Shahani and X. Zheng, "Predicting Backbreak due to Blasting Using LSSVM Optimized by Metaheuristic Algorithms," *Environmental Earth Sciences* 84, no. 6 (2025): 156, https://doi.org/10.1007/s12665-025-12170-y.

31. E. Ghasemi, H. B. Amnieh, and R. Bagherpour, "Assessment of Backbreak due to Blasting Operation in Open Pit Mines: a Case Study," *Environmental Earth Sciences* 75, no. 7 (2016): 1–11, https://doi.org/10.1007/s12665-016-5354-6.

32. A. Saghatforoush, M. Monjezi, R. Shirani Faradonbeh, and D. Jahed Armaghani, "Combination of Neural Network and Ant Colony Optimization Algorithms for Prediction and Optimization of Flyrock and back-break Induced by Blasting," *Engineering With Computers* 32, no. 2 (2016): 255–266, https://doi.org/10.1007/s00366-015-0415-0.

33. S. Kumar, A. Mishra, and B. Choudhary, "Prediction of Back Break in Blasting Using Random Decision Trees," *Engineering With Computers* 38, no. Suppl 2 (2022): 1185–1191, https://doi.org/10.1007/s00366-020-01280-9.

34. T. Long, M. Akbari, and P. Fakharian, "Prediction of Soil Liquefaction Using a Multi-Algorithm Technique: Stacking Ensemble Techniques and Bayesian Optimization," *Journal of Soft Computing in Civil Engineering* (2024): 33–56.

35. K. C. Onyelowe, D. R. Eidgahee, H. Jahangir, F. I. Aneke, and L. I. Nwobia, "Forecasting Shear Parameters, and Sensitivity and Error Analyses of Treated Subgrade Soil," *Transportation Infrastructure Geotechnology* 10, no. 3 (2023): 448–473, https://doi.org/10.1007/s40515-022-00225-7.

36. V. Abdi, *File:Sungun Copper Mine 2019-08-13 04.jpg* (Wikimedia Commons, 2019).

37. T. Nasrabadi, G. Nabi Bidhendi, A. Karbassi, et al., "Influence of Sungun Copper Mine on Groundwater Quality, NW Iran," *Environmental Geology* 58, no. 4 (2009): 693–700, https://doi.org/10.1007/s00254-008-1543-2.

38. A. A. Kamali, M. Moayyed, N. Amel, et al., "Mineralogy, Mineral Chemistry and Thermobarometry of Post-mineralization Dykes of the Sungun Cu–Mo Porphyry Deposit (Northwest Iran)," *Open Geosciences* 12, no. 1 (2020): 764–790, https://doi.org/10.1515/geo-2020-0009.

39. S. Hassanpour, "The Sungun Porphyry Magma Resource and the 120,000-year Difference in Age Between the Main Stock and the First Dike: New Evidence from 87Sr/86Sr, 143Nd/144Nd and Pb, SHRIMP U–Pb Zircon Dating in NW Iran," *Iranian Journal of Earth Sciences* 9, no. 2 (2017): 94–104.

40. M. Seyedali and L. Andrew, *The Whale Optimization Algorithm Advances in Engineering Software* (Amsterdam, The Netherlands: Elsevier Ltd, 2016).

41. W. A. Watkins and W. E. Schevill, "Aerial Observation of Feeding Behavior in Four Baleen Whales: Eubalaena glacialis, Balaenoptera borealis, Megaptera novaeangliae, and Balaenoptera physalus," *Journal of Mammalogy* 60, no. 1 (1979): 155–163, https://doi.org/10.2307/1379766.

42. J. A. Goldbogen, A. S. Friedlaender, J. Calambokidis, M. F. Mckenna, M. Simon, and D. P. Nowacek, "Integrative Approaches to the Study of Baleen Whale Diving Behavior, Feeding Performance, and Foraging Ecology," *BioScience* 63, no. 2 (2013): 90–100, https://doi.org/10.1525/bio.2013.63.2.5.

3148, 2026, 1, Downloaded from https://onlinelibrary.wiley.com/doi/10.1155/vib/4973137 by National Health And Medical Research Council, Wiley Online Library on [18/11/2026]. See the Terms and Conditions (https://onlinelibrary.wiley.com/terms-and-conditions) on Wiley Online Library for rules of use; OA articles are governed by the applicable Creative Commons License

43. Q. M. GuolinKe, T. Finley, T. Wang, et al., "Lightgbm: a Highly Efficient Gradient Boosting Decision Tree," *Advances in Neural Information Processing Systems* 30 (2017): 52.

44. X. Wen, Y. Xie, L. Wu, and L. Jiang, "Quantifying and Comparing the Effects of Key Risk Factors on Various Types of Roadway Segment Crashes with LightGBM and SHAP," *Accident Analysis & Prevention* 159 (2021): 106261, https://doi.org/10.1016/j.aap.2021.106261.

45. K. Li, H. Xu, and X. Liu, "Analysis and Visualization of Accidents Severity Based on LightGBM-TPE," *Chaos, Solitons & Fractals* 157 (2022): 111987, https://doi.org/10.1016/j.chaos.2022.111987.

46. C. Gokceoglu, C. Bal, and C. H. Aladag, "Modeling of Tunnel Boring Machine Performance Employing Random Forest Algorithm," *Geotechnical & Geological Engineering* 41, no. 7 (2023): 4205–4231, https://doi.org/10.1007/s10706-023-02516-3.

47. X. Kong, X. Ling, L. Tang, W. Tang, and Y. Zhang, "Random Forest-based Predictors for Driving Forces of Earth Pressure Balance (EPB) Shield Tunnel Boring Machine (TBM)," *Tunnelling and Underground Space Technology* 122 (2022): 104373, https://doi.org/10.1016/j.tust.2022.104373.

48. H. Xie, J. Dong, Y. Deng, and Y. Dai, "Prediction Model of the Slope Angle of Rocky Slope Stability Based on Random Forest Algorithm," *Mathematical Problems in Engineering* 2022, no. 1 (2022): 9441411–10, https://doi.org/10.1155/2022/9441411.

49. Y. Lin, K. Zhou, and J. Li, "Prediction of Slope Stability Using Four Supervised Learning Methods," *IEEE Access* 6 (2018): 31169–31179, https://doi.org/10.1109/access.2018.2843787.

50. S. S. Matin, L. Farahzadi, S. Makaremi, S. C. Chelgani, and G. H. Sattari, "Variable Selection and Prediction of Uniaxial Compressive Strength and Modulus of Elasticity by Random Forest," *Applied Soft Computing* 70 (2018): 980–987, https://doi.org/10.1016/j.asoc.2017.06.030.

51. C. Yuan, H. Zhang, L. Wang, et al., "Research on Strength Prediction of Crack Rock Mass Based on Random Forest Algorithm," *Bulletin of Engineering Geology and the Environment* 83, no. 4 (2024): 128, https://doi.org/10.1007/s10064-024-03629-6.

52. X. Ma, Z. Chen, P. Chen, et al., "Predicting the Utilization Factor of Blasthole in Rock Roadways by Random Forest," *Underground Space* 11 (2023): 232–245, https://doi.org/10.1016/j.undsp.2023.01.006.

53. S. Lin, Z. Liang, S. Zhao, M. Dong, H. Guo, and H. Zheng, "A Comprehensive Evaluation of Ensemble Machine Learning in Geotechnical Stability Analysis and Explainability," *International Journal of Mechanics and Materials in Design* 20, no. 2 (2024): 331–352, https://doi.org/10.1007/s10999-023-09679-0.

3148, 2026, 1, Downloaded from https://onlinelibrary.wiley.com/doi/10.1155/vib/4973137 by National Health And Medical Research Council, Wiley Online Library on [18/11/2026]. See the Terms and Conditions (https://onlinelibrary.wiley.com/terms-and-conditions) on Wiley Online Library for rules of use; OA articles are governed by the applicable Creative Commons License